Supplementary Materials:

Impact of Biomass Burning Organic Aerosol Volatility on Smoke Concentrations Downwind of Fires

Demetrios Pagonis,[1,2,3,*] Vanessa Selimovic,[4,a] Pedro Campuzano-Jost,[1,2] Hongyu Guo,[1,2] Douglas A. Day,[1,2] Melinda K. Schueneman,[1,2] Benjamin A. Nault,[1,2,b] Matthew M. Coggon,[5] Joshua P. DiGangi,[6] Glenn S. Diskin,[6] Edward C. Fortner,[7] Emily M. Gargulinski,[8] Georgios I. Gkatzelis,[2,5,c] Johnathan W. Hair,[6] Scott C. Herndon,[7] Christopher D. Holmes,[9] Joseph M. Katich,[2,5,d] John B. Nowak,[6] Anne E. Perring,[10] Pablo Saide,[11,12] Taylor J. Shingler,[6] Amber J. Soja,[6] Laura H. Thapa,[11] Carsten Warneke,[5] Elizabeth B. Wiggins,[6] Armin Wisthaler,[13,14] Tara I. Yacovitch,[7] Robert J. Yokelson,[4] and Jose L. Jimenez[1,2,*]

[1]Department of Chemistry, University of Colorado Boulder, Boulder, CO 80309, USA
[2]Cooperative Institute for Research in Environmental Sciences (CIRES), University of Colorado, Boulder 80309 CO, USA
[3]Department of Chemistry and Biochemistry, Weber State University, Ogden 84408 Utah, USA
[4]Department of Chemistry, University of Montana, Missoula, MT 59812, USA
[5]NOAA Chemical Sciences Laboratory, Boulder, CO 80305, USA
[6]NASA Langley Research Center, Hampton, VA 23666, USA
[7]Aerodyne Research, Inc., Billerica, MA 01821, USA
[8]National Institute of Aerospace, Hampton, VA 23666, USA
[9]Florida State University Department of Earth, Ocean and Atmospheric Science, Tallahassee, FL 32304, USA
[10]Department of Chemistry, Colgate University, Hamilton, NY 13346, USA
[11]Department of Atmospheric and Oceanic Sciences, University of California, Los Angeles, Los Angeles, CA 90095, USA
[12]Institute of the Environment and Sustainability, University of California, Los Angeles, Los Angeles, CA 90095, USA
[13]Department of Chemistry, University of Oslo, 0371 Oslo, Norway
[14]Institut für Ionenphysik und Angewandte Physik, Universität Innsbruck, 6020 Innsbruck, Austria

Now at:
[a]Department of Chemistry, University of Michigan, Ann Arbor, MI 48109
[b]Center for Aerosol and Cloud Chemistry, Aerodyne Research, Inc., Billerica, MA 01821, USA and Department of Environmental Health and Engineering, The Johns Hopkins University, Baltimore, MD 21218, USA
[c]Institute of Energy and Climate Research, IEK-8: Troposphere, Forschungszentrum Jülich GmbH, 54245 Jülich, Germany
[d]Ball Aerospace, Boulder, CO 80301, USA

Correspondence: Demetrios Pagonis: demetriospagonis@weber.edu and Jose L. Jimenez: jose.jimenez@colorado.edu

Prepared for *Environmental Science & Technology*

Summary of Contents:

This supplement is twenty-four pages long and contains the following sections, tables, and figures:

Table S1. *North American wildfire studies used in this manuscript's analysis*

Study Name	Year	Platform	Fire Type	Location(s)	No. Fire-Days Sampled	PM Instrumentation	References
FIREX-AQ	2019	Airborne, NASA DC-8	Wildland	CA, ID, MT, UT, WA	19	High-resolution aerosol mass spectrometer (HR-AMS);[1-3] Extractive electrospray ionization mass spectrometer (EESI-TOF)[4]	[5]
FIREX-AQ	2019	Airborne, NASA DC-8	Agricultural	AL, AR, FL, GA, IL, KS, LA, MO, MS, NE, OK, TX	79	HR-AMS EESI-TOF	[5]
WE-CAN	2018	Airborne, NSF/NCAR C-130	Wildland	CA, CO, ID, MT, NV, OR, UT, WA	13	HR-AMS	[6,7]
BBOP	2013	Airborne, DOE G-1	Wildland	CA, OR, WA	14	Soot-particle high-resolution aerosol mass spectrometer[8]	[9]
BBOP	2013	Fixed ground site, high-altitude (2.8 km)	Wildland	Mount Bachelor Observatory, OR	18	HR-AMS	[9]
SEAC^{4}RS	2013	Airborne, NASA DC-8	Wildland	CA, OR, WA	2	HR-AMS	[10]
SEAC^{4}RS	2013	Airborne, NASA DC-8	Agricultural	AR, MO, MS, LA	13	HR-AMS	[11]
MSO	2017	Fixed ground site	Wildland	Missoula, MT	24	Environmental beta-attenuation mass monitor [10]	[12]
MSO	2018	Fixed ground site	Wildland	Missoula, MT	18	Environmental beta-attenuation mass monitor	[13]
WE-CAN	2018	Ground, Aerodyne mobile laboratory	Wildland	ID, WA	3	HR-AMS	
FIREX-AQ	2019	Ground, Aerodyne mobile laboratory	Wildland	AZ, ID, WA	24	HR-AMS	

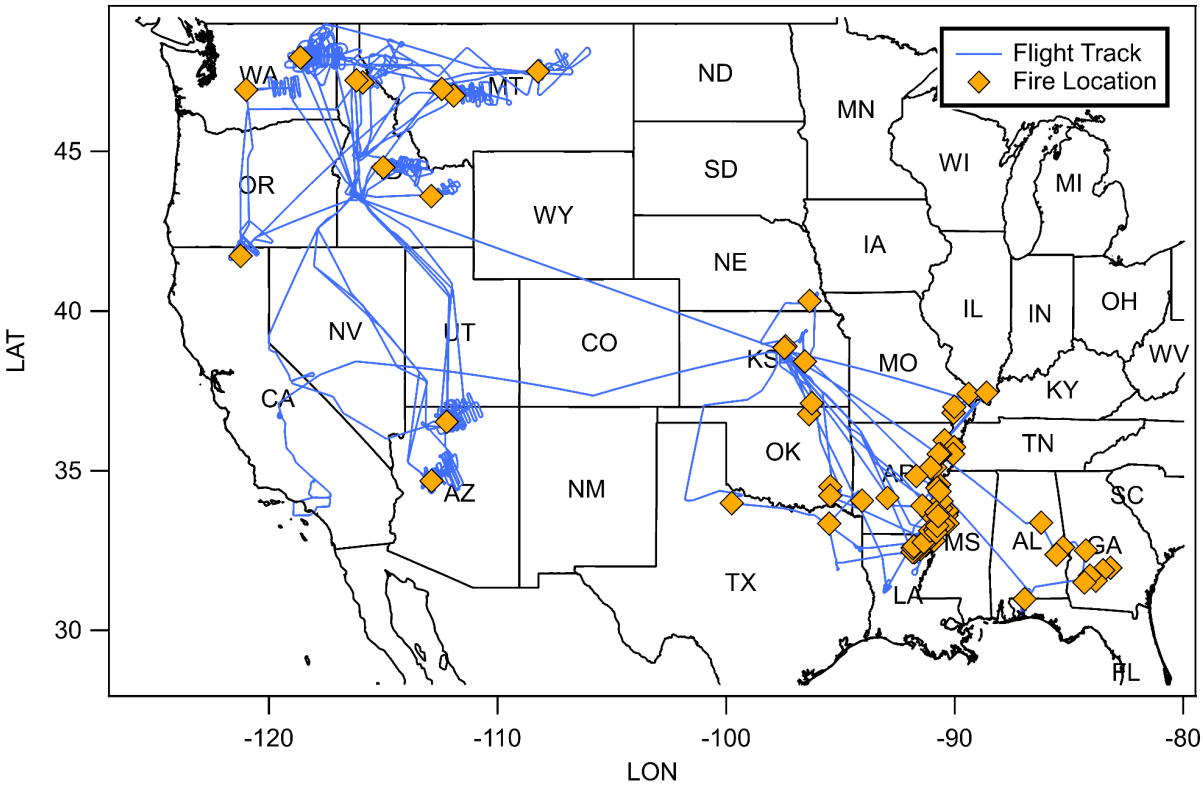

Figure S1. *Flight track and fire locations for the NASA DC-8 FIREX-AQ deployment. Additional campaign, instrumentation and fire details are available in Warneke et al.*[5]

Section SI-I: Calculation of NEMRs

Normalized excess mixing ratios (NEMRs) that were determined in this work were determined as follows. For FIREX-AQ airborne measurements we determined background concentrations as one-minute averages before and after each plume transect and interpolating across the transect. AML data was defined as smoke-impacted when the HCN:CO ratio exceeded 0.002 and PM NEMR was then calculated using linear regression.

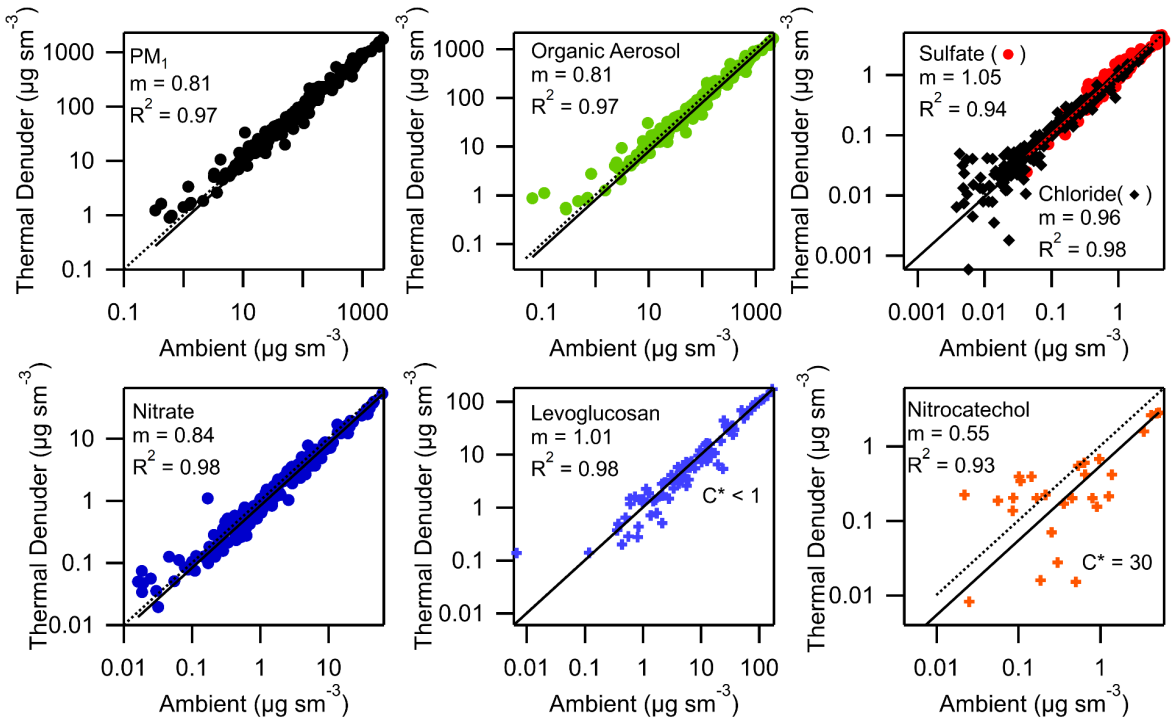

Figure S2. *Same as Figure 2, but in log scale. Organic aerosol, nitrate, and nitrocatechol demonstrate measurable evaporation while aerosol sulfate, chloride, and levoglucosan do not evaporate within the measurement uncertainties.*

Section SI-II: ***Thermal Denuder Analysis***

Relating the concentrations of species measured at the exit of the thermal denuder (TD) to the ambient concentrations of those species requires a full treatment of the interaction between the changes in ambient concentrations of smoke compounds (significant minute-to-minute variability) with the residence time of the TD (median 90 s). The following sections describe that analysis.

TD Residence Time

Flow inside the TD is not perfectly laminar due to the rapid jump from the 0.5 cm inner diameter tubing to the 22 cm diameter TD. The residence time distribution of the TD was measured using rapid pulsed injections of ammonium sulfate aerosol during FIREX-AQ maintenance days. Ammonium sulfate at the exit of the TD was measured with the AMS. Example data from a single ammonium sulfate injection and the average cumulative residence time distribution during the campaign are shown in Fig. S3 below.

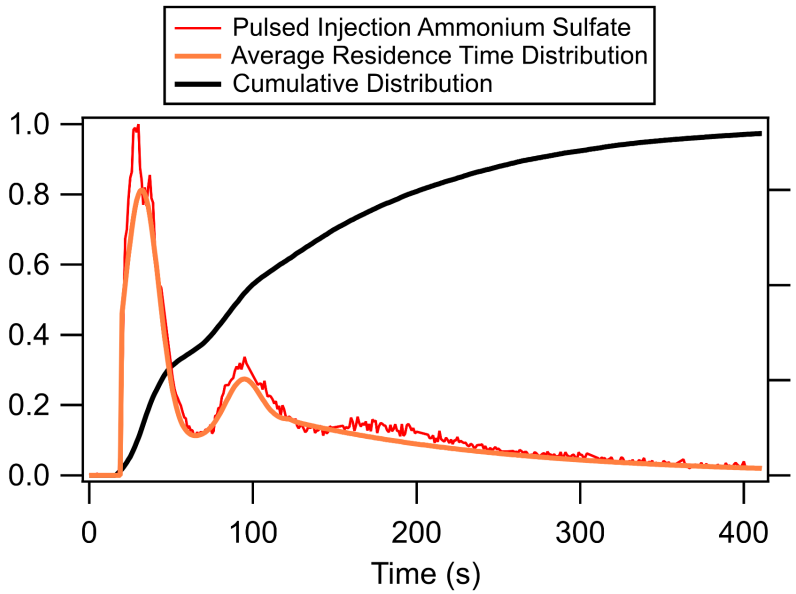

Figure S3. *The average residence time distribution measured for the TD used in this study, along with an example normalized time series of a single pulsed injection and the cumulative residence time distribution.*

Gaps In AMS and EESI-MS Duty Cycle

Both the AMS and EESI-MS time series of ambient aerosol concentrations contain regular data gaps from times spent measuring instrument background, aerosol size distributions, and sampling from the TD. The AMS duty cycle has gaps in the ambient time series roughly every minute for these other measurements. For a typical FIREX-AQ semi-lagrangian sampling pattern with TD sampling these gaps represent 31% and 21% of the AMS and EESI-MS time series, respectively. In order to fully quantify the interactions between the ambient time series and the TD residence time distribution we must fill those data gaps with an estimate of the ambient concentration. This interpolation is done by calculating the correlation (orthogonal distance regression) of the analyte with CO in the 5 minutes preceding and following each data gap, and then calculating the interpolated value from the 1-second CO time series. The variability in NEMR across 5-minute time gaps is small, and the interpolated regions are largely indistinguishable from ambient data in the time series (Fig S4).

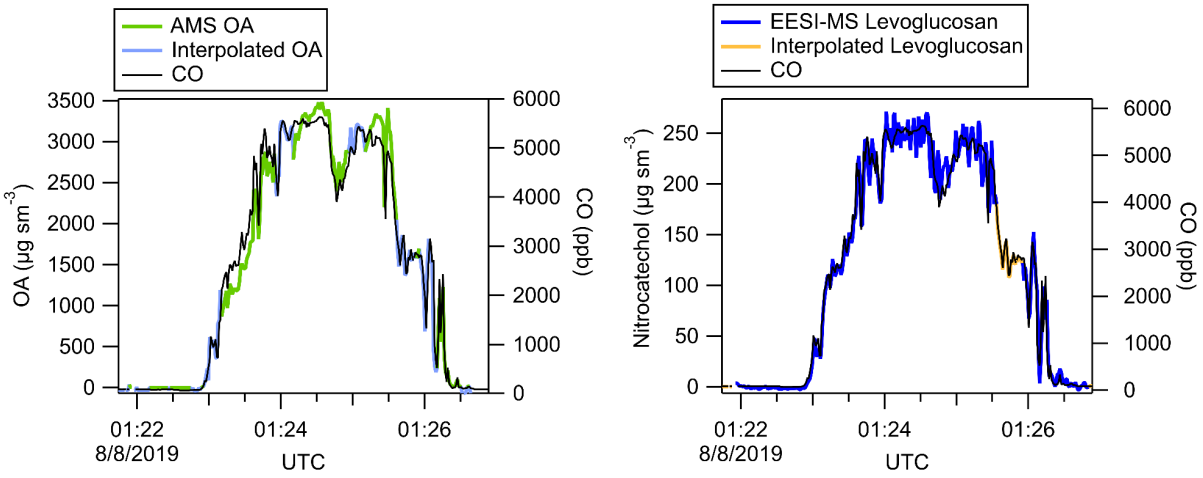

Figure S4. *Interpolated AMS OA and EESI-MS levoglucosan overlaid with DACOM CO to show plume structure.*

Convolving Ambient Variability and Thermal Denuder Residence Time

In the absence of any evaporation, the time series of a species exiting the TD can be calculated as the convolution of the ambient time series with the residence time distribution of the TD, as follows:

$$TD(t) = A(t) * I(t) = \int_0^\infty [A(t-\tau) \times I(\tau)]\, d\tau \quad \text{(S1)}$$

Where *TD(t)* is the time series at the exit of the TD, *A(t)* is the ambient time series of the species, *I(t)* is the TD response function (1 - cumulative residence time distribution). The calculated time series *TD(t)* is then averaged for the time spent sampling the TD, corrected for particle wall loss, and compared to the measured concentration (Fig S5; Fig. 2 of the main text).

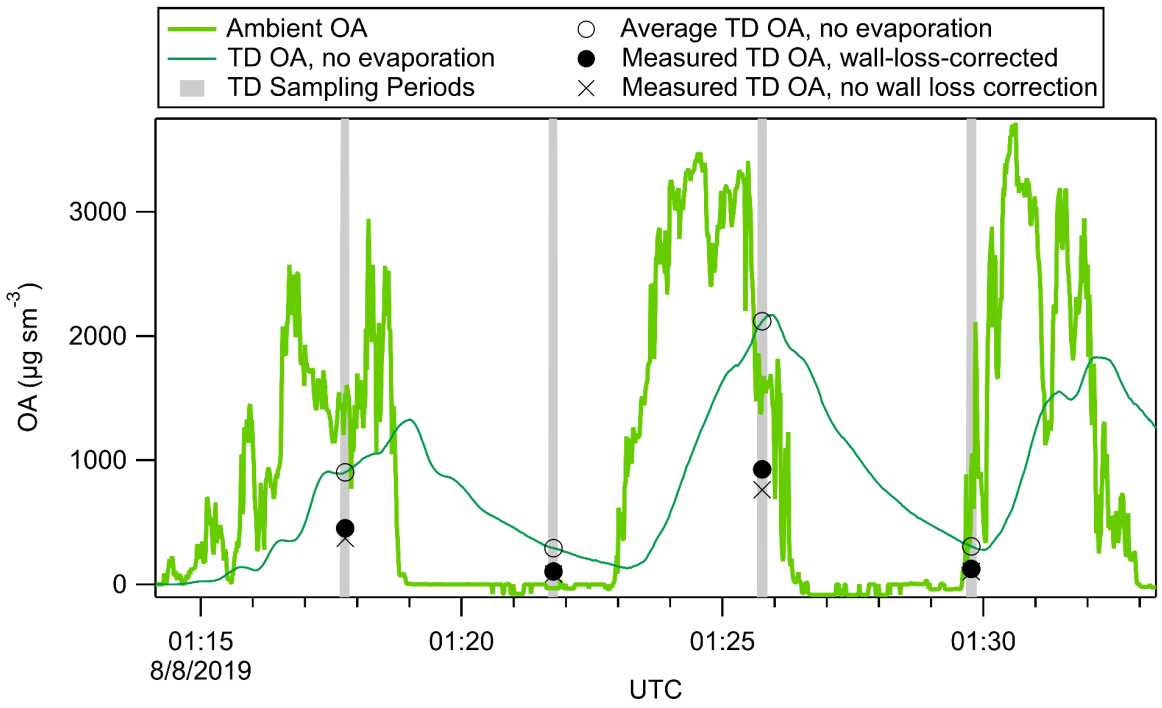

Figure S5. *Time series of ambient OA and OA at the exit of the TD in the absence of evaporation, calculated through convolution of the ambient time series and the residence time distribution of the TD.*

Particle Wall Loss

Wall loss of particles inside the TD affects the relationship between the calculated and measured concentrations at the exit of the TD. In previous airborne deployments of the TD (flown as an oxidation flow reactor during KORUS-AQ), the particle wall loss was determined to be 10%[3] by taking the ratio of ambient and measured sulfate, which was assumed to be non-volatile. In FIREX-AQ we replicate this analysis with two non-volatile species: AMS chloride (predominantly KCl for FIREX-AQ), and AMS inorganic sulfate. Both of these species showed a consistent wall loss fraction, with an average of 24 ± 4% (mean ± range/2) for FIREX-AQ (Fig. S6), and this correction factor is applied to all TD data. While the particle transmission is dependent on the size distribution of the aerosol sampled, the smoke sampled during FIREX-AQ had a consistent size distribution, enabling us to apply a single correction factor for the entire campaign.[14] All other species in the AMS and EESI-MS measurements are expected to evaporate to some extent, and all species show greater losses than AMS sulfate and chloride. We interpret all loss in excess of the particle wall loss fraction to be due to evaporation. The flow rate of the TD was higher during FIREX-AQ (6.3 L min^{-1}) compared to KORUS-AQ (5.2 lpm) in order to accommodate the sampling needs of the EESI-MS. We tentatively attribute the higher particle wall loss in FIREX-AQ to this increase in flow rate inside the TD.

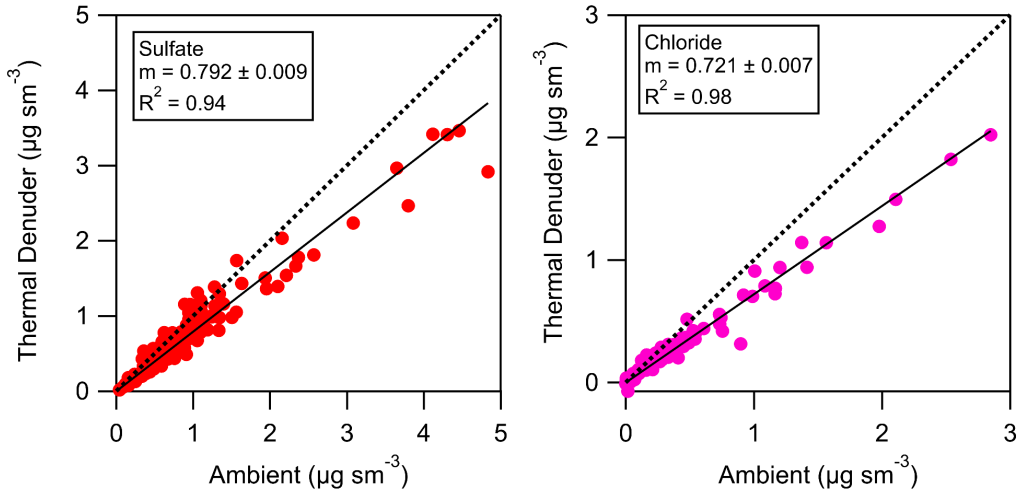

Figure S6. *Uncorrected TD measurements of two non-volatile species measured by the AMS. Displayed uncertainty in slope is the fit uncertainty (1 σ). The wall loss correction factor applied in this study is the average of the two slopes: 0.757.*

Section SI-III: ***Evaluation of Literature and Fitting of BBOA VBS***

BBOA volatility basis sets from the literature were evaluated by using each VBS as an input to the kinetic evaporation model of Cappa[15] and comparing the output mass fraction remaining (MFR) to the measured MFR for each TD data point. The VBS's evaluated and the sum of squared MFR residuals is presented in Table S2.

The VBS of May et al. (2013) is the best-performing basis set from the literature. This VBS was determined using TD measurements of all burns during FLAME III, which were selected to represent common fuels found in the Western United States. Other VBS presented below are derived from modeling studies, burns of single fuel types, or bottom-up estimates. Given the ever-present risk of overfitting data when deriving a VBS, we encourage future studies to include the May et al. VBS in their analysis, since we do not know if it is more representative of wildfire smoke than the FIREX-AQ dataset. We include a 'flat' VBS to illustrate the limitations of this brute-force fitting. Assuming an even distribution of mass across an arbitrary volatility range performs quite well.

Table S2. *Summary of literature volatility basis set evaluation against the FIREX-AQ TD data. Table is ordered by increasing sum of squared residuals (SSR). Fitted MFR for the TD measurements is 0.81.*

VBS		**Fitted MFR**	**MFR SSR**

Fitted, this work	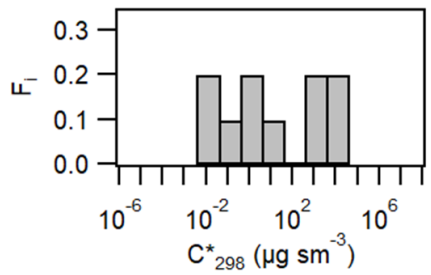	0.70	5.1
Flat	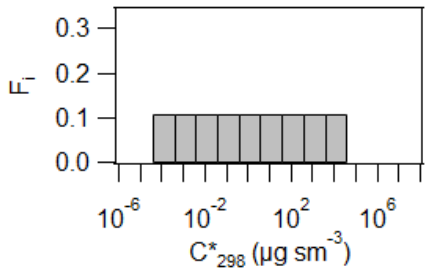	0.69	7.4
May et al. 2013[16]	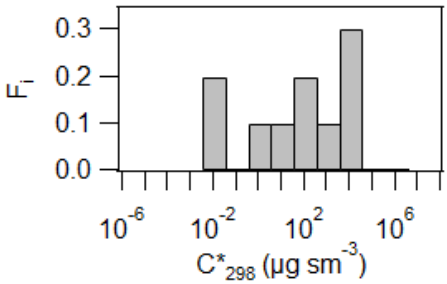	0.57	11.6
Shingler et al. 2016[17]	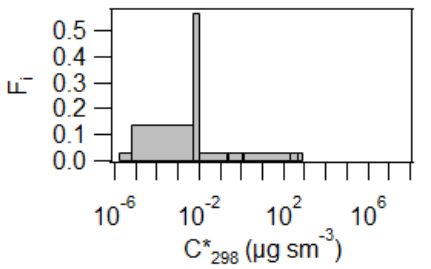	0.93	11.6
Theodoritsi et al. 2021[18]	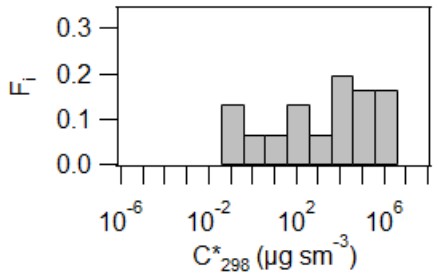	0.51	16

Hatch et al. 2018[19]	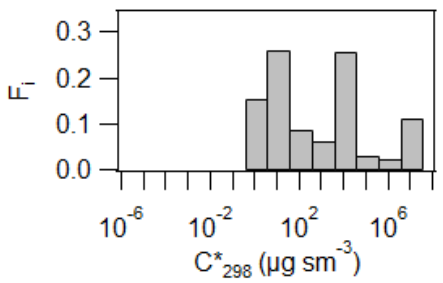	0.60	28
Cappa and Jimenez 2010[20]	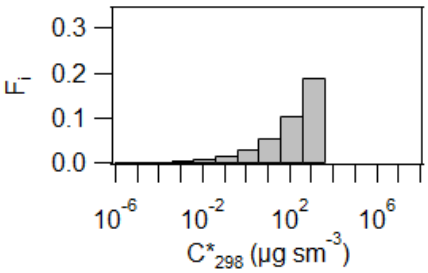	0.30	54

Fitting of Volatility Basis Set

A BBOA volatility basis set was fitted to this study's TD measurements so that the measurements could be applied generally in a model like HRRR-Smoke. Following preliminary investigation of the literature VBS presented above, we carried out a brute-force fit, following the methodology of May et al.[16] Volatility range (C^*_{298}) was constrained from 10^{-2}–10^{4} µg m^{-3}, enthalpy of vaporization was calculated using the parameterization of May et al. (2013). The amount of VBS mass within each bin was varied across four different levels (e.g. 0, 1, 2, 3) and then normalized. Sum of squared residuals of each VBS was evaluated against the measured MFR from the FIREX-AQ TD measurements. The best-performing VBS is presented in the table above. Since the TD was at constant temperature, our TD results are insensitive to changes in ΔH_{vap}, and using varied parameterizations from the literature did not meaningfully affect the SSR or slope of the optimal fitted VBS.

OA Evaporation Kinetic Model

The kinetic evaporation model used in this work is adapted from that of Cappa,[15] with the only modification being the removal of the radial dependence of evaporation rate. This model assumes a mass accommodation coefficient of unity. This assumption is likely not perfect for all species across all TD measurements during FIREX-AQ, but the empirical observation of significant evaporation inside the TD shows that there are not large mass transport limitations for BBOA evaporation at 40-45 °C. This is consistent with laboratory measurements of mass accommodation coefficients for SVOC condensing to a diverse set of aerosols.[21] Additionally, any kinetic barrier to evaporation in the TD would cause our derived VBS to appear less volatile than the true volatility distribution of BBOA. Accordingly, this assumption limits the extent of

evaporation predicted for our VBS and does not affect our conclusion that gas-particle partitioning is a major driver of BBOA NEMR.

We run this model with a volatility basis set as the input, calculating C*, condensation, and evaporation rates as the aerosol is heated inside the inlet and TD. The evaporation time series for different C* bins are shown in Fig. S7. The rate and extent of evaporation increases with C*, with the most volatile components of OA evaporating fastest.

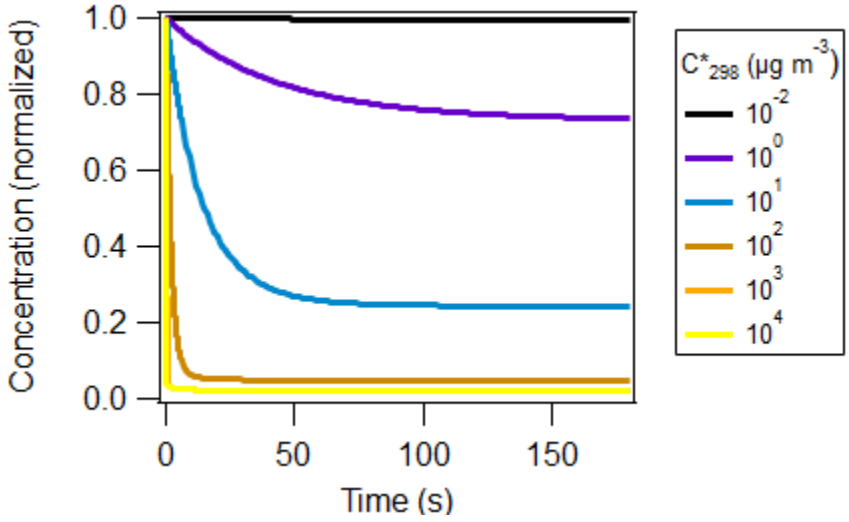

Figure S7. *Evaporation time series for the volatility bins of the May et al. (2013) VBS in the TD model used in this study. Model output is for 100 μg sm^{-3} of OA at an ambient temperature of 10 ℃ and a denuder temperature of 40 ℃.*

Use of Median Residence Time for Model Calculations

Because there is a statistical distribution of residence times for particles inside the TD and the evaporation is kinetically limited, not all particles passing through the TD undergo the same extent of evaporation. This challenges our attempts to model aerosol evaporation with VBS inputs, because we seek to calculate a single MFR for a given input concentration. To arrive at a single value of MFR, we calculate MFR at the median residence time of the TD (90 s). Particles exiting the TD ahead of the median residence time will have a higher MFR than those exiting after the median residence time, and we assume that these competing effects cancel out. Fully accounting for this bias in the campaign-wide modeling is computationally slow, and we show in Fig. S8 that this assumption is good to within 2% across the range of OA concentrations studied in FIREX-AQ. This assumption performs worst at approximately 60 μg sm^{-3} of OA, where MFR is biased downwards by 1.8% (0.545 vs 0.554). The mass fraction remaining time series of this worst-case scenario is shown in Fig. S8A, and the source of the bias can be seen in the mass exiting the TD from 20-50 seconds, which has a slightly higher MFR than mass exiting at the median residence

time (90 s). At high OA concentrations the majority of the evaporated mass is at a sufficiently high volatility that it is lost within seconds, as shown in Figure S7 above.

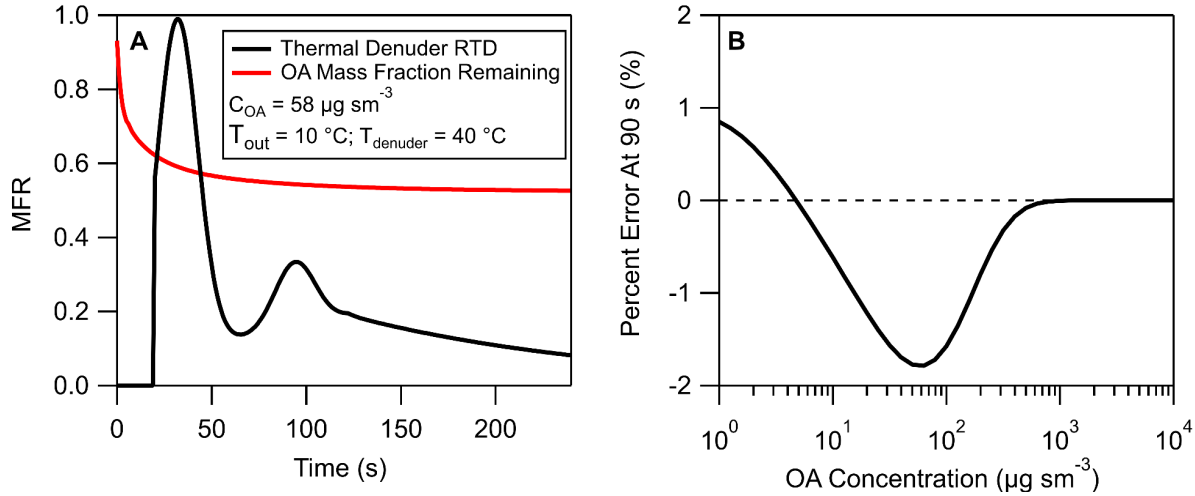

Figure S8. *Thermal denuder residence time distribution and OA mass fraction remaining for typical sampling conditions (A), and the percent error introduced in the MFR calculations by using the value at the median residence time (90 s) instead of a full treatment of the interplay between residence time and evaporation kinetics (B). The conditions used to model MFR in (A) are those giving the highest error in (B).*

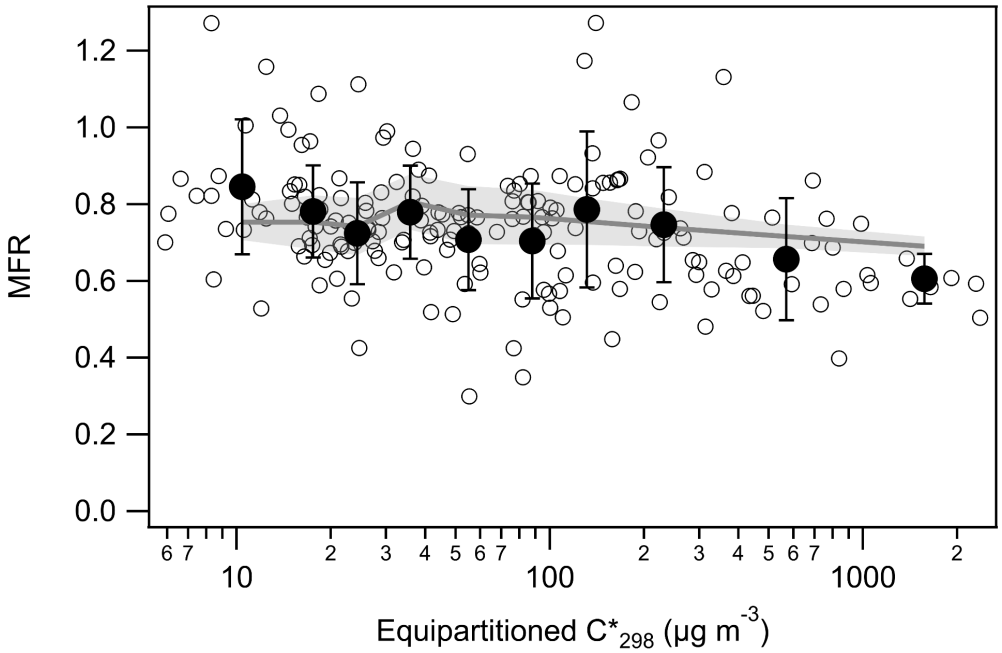

Figure S9. *Dependence of the mass fraction remaining (MFR) of thermally denuded OA as a function of equipartitioned C*$_{298}$ (defined below). As expected, when partitioning favors the particle phase (higher Equipartitioned C*$_{298}$) the extent of evaporation is greatest.*

Section SI-IV: ***Sheridan Fire Plume Dynamics***

To better understand the injection dynamics of the Sheridan Fire plume from August 15th, 2019 we utilized WRF-CHEM output to calculate back-trajectories of the smoke plume. Figure S10 shows the back trajectories for the hour prior to sampling for several points along the plume transect, projected onto the vertical plane containing the flight path. Overall, these results suggest that the plume was initially lofted, and then smoke descended. While useful for understanding the evolution of the smoke plume, the results presented in the manuscript do not depend on the plume having descended. Our results are unaffected if the early stages of the plume were lofted to lower altitudes than the later emissions.

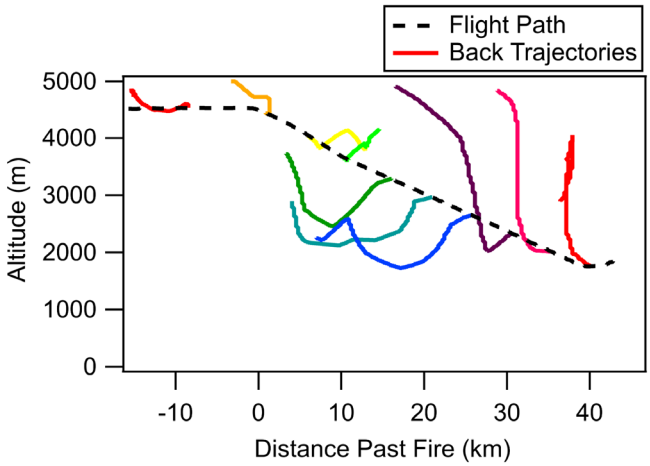

Figure S10. *Back-trajectories of air parcels in the Sheridan Fire plume, calculated from WRF-CHEM wind fields. While this approach has many flaws and is overly simplistic, it does indicate that our interpretation of the Sheridan plume lofting and then subsiding is plausible.*

Section SI-V: ***Emission Factors***

The emission factor of BBOA for each plume transect was calculated using a carbon balance approach[22] with an assumed fuel carbon fraction (F_c) of 0.5. All species used to calculate the carbon balance are presented in Table S3, along with measurement details and the average contribution of the species to the total carbon concentration during FIREX-AQ.

Table S3. *Carbon-containing species used to compute a carbon balance for each smoke plume transect in FIREX-AQ.*

Species	Measurement / Analysis	FIREX-AQ Data Archive ID(s)	Contribution to carbon budget (%)	Always included in calculation
CO_2; carbon dioxide	NASA LICOR 7000, and Plume Ratios	DACOM Plume-Ratios	85	Yes
CO; carbon monoxide	NASA Differential Absorption Carbon monOxide Measurement (DACOM)	DACOM	8.5	Yes
VOC; volatile organic compounds	NOAA Proton-Transfer-Reaction Mass Spectrometer (PTR-MS) University of Oslo PTR-MS[a]	NOAAPTR-VOCs-1Hz PTRMS-NMHC-1Hz	3.2	Yes
OA; organic aerosol	University of Colorado Boulder Aerosol Mass Spectrometer (AMS)	AMS	2.0	Yes
CH_4; methane	NASA Differential Absorption Carbon monOxide Measurement (DACOM)	DACOM	0.9	No
CH_2O; formaldehyde	NASA In Situ Airborne Formaldehyde (ISAF)	ISAF-CH2O-1Hz	0.2	No
C_2H_6; ethane	University of Colorado Boulder Compact Atmospheric Multispecies Spectrometer (CAMS)	C2H6	0.16	No
BC; black carbon	NOAA Single Particle Soot Photometer (SP2)	SP2-BC-1Hz	0.05	No

[a]For the August 7th, 2019 flight total VOCs from the University of Oslo PTR-MS were used since data from the NOAA PTR-MS was unavailable.

Table S3 also details whether we still report an emission factor in the event that concentration data for a single compound is unavailable. If a species contributed more than 1% of the carbon budget on average, then we consider it "necessary" to calculating emission factors. Compounds contributing less than this threshold are omitted from the calculation when data is unavailable. This screening procedure allows us to calculate OA emission factors for 489 of 538 FIREX-AQ plume transects. For calculating the excess CO_2 concentration in each plume we utilize the emission ratio slope product produced and posted to the FIREX-AQ data archive[23] by Hannah Halliday (EPA). This analysis utilizes fully weighted York regressions to calculate the emission ratio across an entire plume transect. We find that utilizing this data product provides the best

accounting of emission ratios, evaluated in terms of how many plumes had calculable (non-negative) emission factors. For OA we use the measured OA to organic carbon (OC) ratio data product from our AMS to convert the OA mass concentration to a carbon concentration. The carbon fraction is assumed to be 1 for black carbon.

The emission factor of OA (EF_{OA}) is calculated from the total carbon concentration (C_C) using the following equation

$$EF_{OA} = C_{OA} \times \chi_C \times 1000 / C_C$$

Where C_{OA} is the mass concentration of OA in the plume, C_C is the total mass concentration of carbon calculated using the species listed above, χ_C is the assumed carbon fraction in the fuels combusted, and the factor of 1000 scales to units of g kg^{-1}.

BBOA Emission Factors by Fuel Type

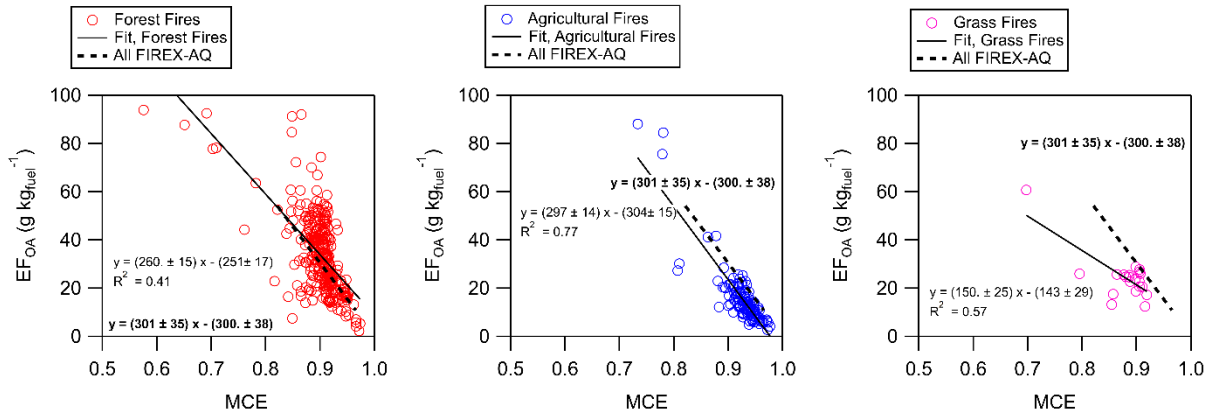

Figure S11. *MCE dependence of the OA emission factor calculated for forest, agricultural, and grass fires.*

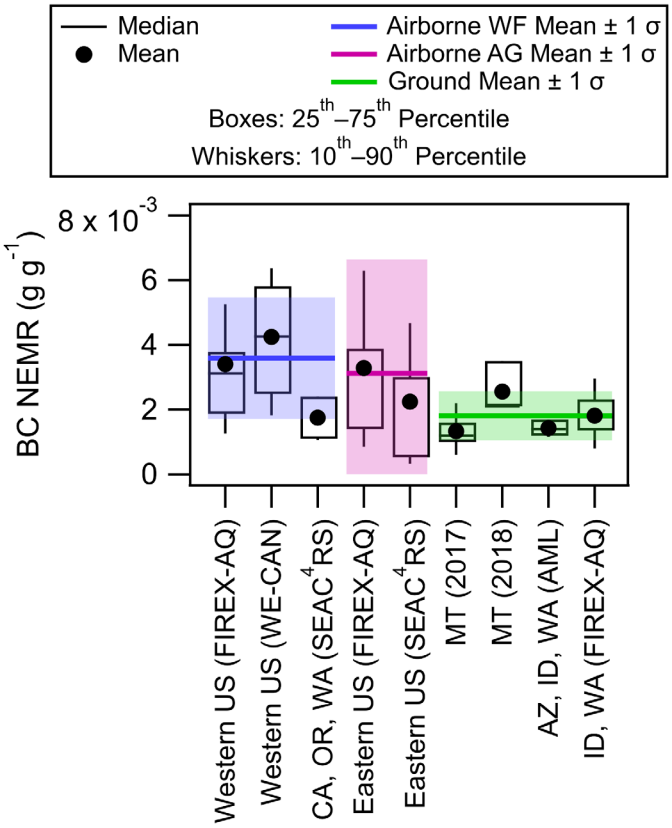

Figure S12. *Campaign-averaged black carbon (BC) NEMRs for the studies included in this analysis. Not all campaigns shown in Figure 1 of the text included a BC measurement.*

Section SI-VI: ***Correlation of FIREX-AQ Smoke Age with Temperature***

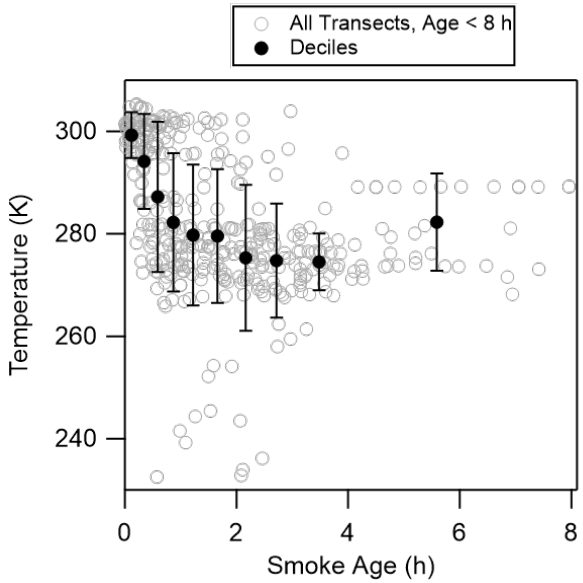

Figure S13. *Smoke age and temperature are correlated in the FIREX-AQ dataset, with 300 K plumes having younger ages than cooler (275 K) plumes. This is largely driven by the fact that plumes could only be tracked across 4+ hours of aging when the plume was large and lofted to several km above the surface. This trend produces an apparent relationship between OA NEMR and smoke age in the FIREX-AQ dataset for the first four hours following emission, since OA has evaporated to a greater extent in the hotter fresh plumes than in the colder, older plumes. When this analysis is restricted to wildland fires the larger trend holds true — with a 7 K decrease in plume temperature from ages 0-2 h, followed by an increase in temp from ages 2-6 h.*

Section SI-VII: ***Emission Factor of SVOCs***

The emission factor of compounds with C^*_{298} below 10^4 μg m^{-3} ($EF_{10,000}$; g kg^{-1}; May et al. 2013[16]) was determined from the OA concentration and the carbon balance described above. The concentration of the VBS ($C_{10,000}$) was adjusted iteratively until the OA concentration of the VBS was equal to the measured OA concentration. The emission factor of the VBS (EF_{VBS}) was then calculated as

$$EF_{VBS} = C_{VBS} \times \chi_C \times 1000 / C_C \quad \text{(S2)}$$

where χ_C is the assumed carbon fraction in the fuels combusted. The campaign average for EF_{VBS} at FIREX-AQ was 41.5 g kg^{-1}. At FLAME III the range of EF_{VBS} values observed varied from 1 to 200 g kg^{-1}, and we observe a similar range of 3 to 148 g kg^{-1}. EF_{VBS} shows a linear dependence with MCE, as shown in Fig. S14, with high-efficiency burns converting less fuel mass to semivolatile compounds.

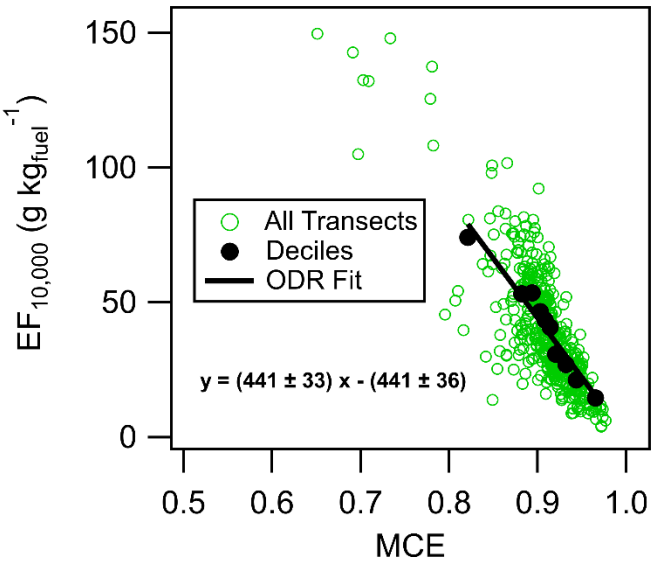

Figure S14. *Correlation of SVOC emission factor with modified combustion efficiency.*

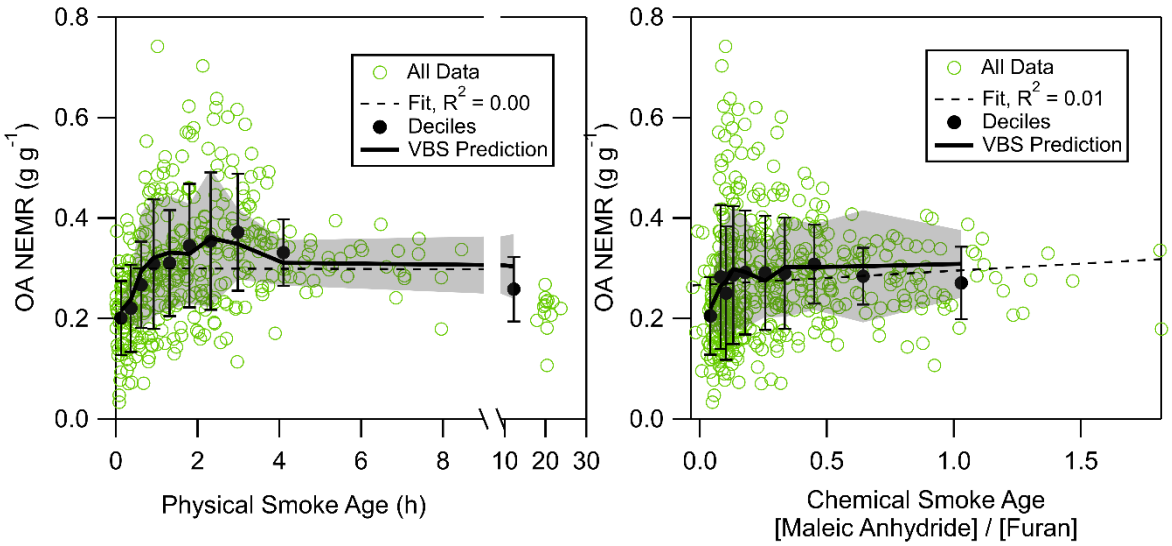

Figure S15. Comparison of OA NEMR trends in the FIREX-AQ dataset as a function of both physical smoke age and chemical smoke age. In both cases the observed variability in OA NEMR is interpreted as being due to changes in partitioning state, as illustrated by the strong correlation between VBS-predicted NEMR and observed NEMR.

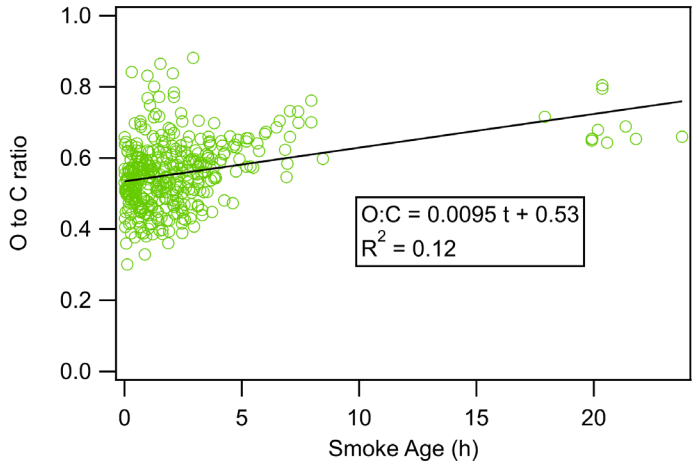

Figure S16. *Relationship between O:C ratio of BBOA and smoke age showing an increase that is potentially due to chemical aging of the smoke.*

Equipartitioned C^*_{298}

The vapor pressure of organic compounds equally partitioned between the gas and particle phase in a given smoke plume is calculated using the plume temperature, pressure, and OA concentration. Note that OA concentration in aircraft studies is typically plotted and reported as micrograms of OA per standard cubic meter (μg sm^{-3}; $C_{OA,std}$; standard T = 273.15, P=1013.25

mbar) while gas-particle partitioning is calculated using volumetric OA concentrations under actual temperature and pressure conditions (μg m^{-3}; $C_{OA,vol}$)

$$C_{OA,vol} = C_{OA,std} \times \frac{273.15}{T} \times \frac{P}{1013.25} \quad \text{(S3)}$$

The equipartitioned C* is then calculated from the following equation[24] where the fraction in the particle phase F_p is set to 0.5.

$$F_p = \left(1 + \frac{C^*_{\mathrm{T}}}{C_{OA,\mathrm{vol}}}\right)^{-1} \quad \text{(S4)}$$

This reduces to $C^*_T = C_{OA,vol}$, where C^*_T is the saturation vapor pressure of equipartitioned compounds at the temperature of the plume. This value must be converted to C^*_{298}, the saturation vapor concentration at 298 K. This is accomplished through the Clausius-Clapeyron relationship

$$C^*_{\mathrm{T}} = C^*_{298} \frac{298}{T} \exp\left(\frac{-\Delta H_{vap}}{R}\left[\frac{1}{298} - \frac{1}{T}\right]\right) \quad \text{(S5)}$$

Where the enthalpy of vaporization ΔH_{vap} (kJ mol^{-1}) of a compound is dependent on C^*_{298} according to the following relationship[16]

$$\Delta H_{vap}\ (kJ\ mol^{-1}) = 85 - 4\ log(C^*_{298}) \quad \text{(S6)}$$

This is the relationship underlying the fitted VBS that is used throughout this work, and we utilize it in these calculations to maintain consistency across the manuscript. Equations S5 and S6 must be solved iteratively to simultaneously determine C^*_{298} and ΔH_{vap}. When calculated for all of FIREX-AQ, equipartitioned C^*_{298} shows a higher correlation coefficient with OA NEMR than OA concentration or temperature independently (Fig. S17). This result supports the assumption underlying this work that there is a consistent SVOC:CO emission ratio from fires in the United States.

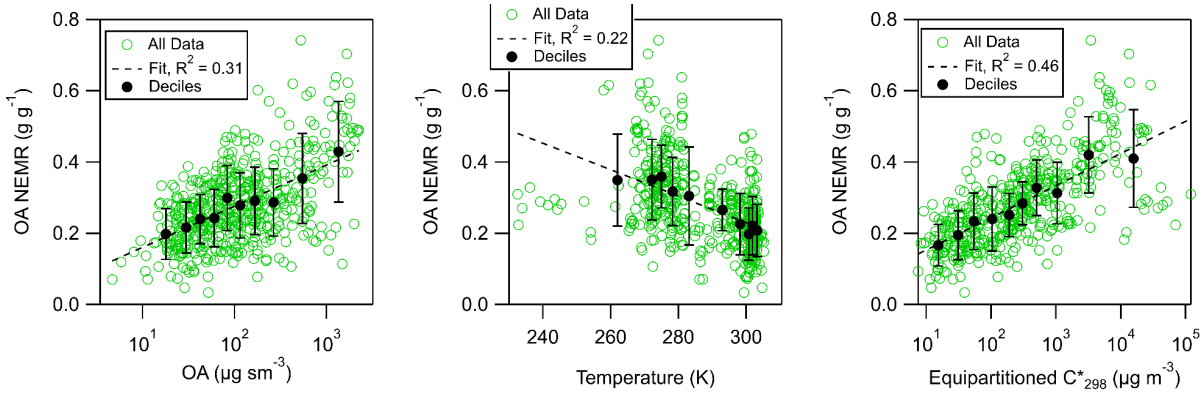

Figure S17. *The equipartitioned C^*_{298} of a plume gives a higher correlation coefficient with OA NEMR than the two input parameters of OA concentration and temperature.*

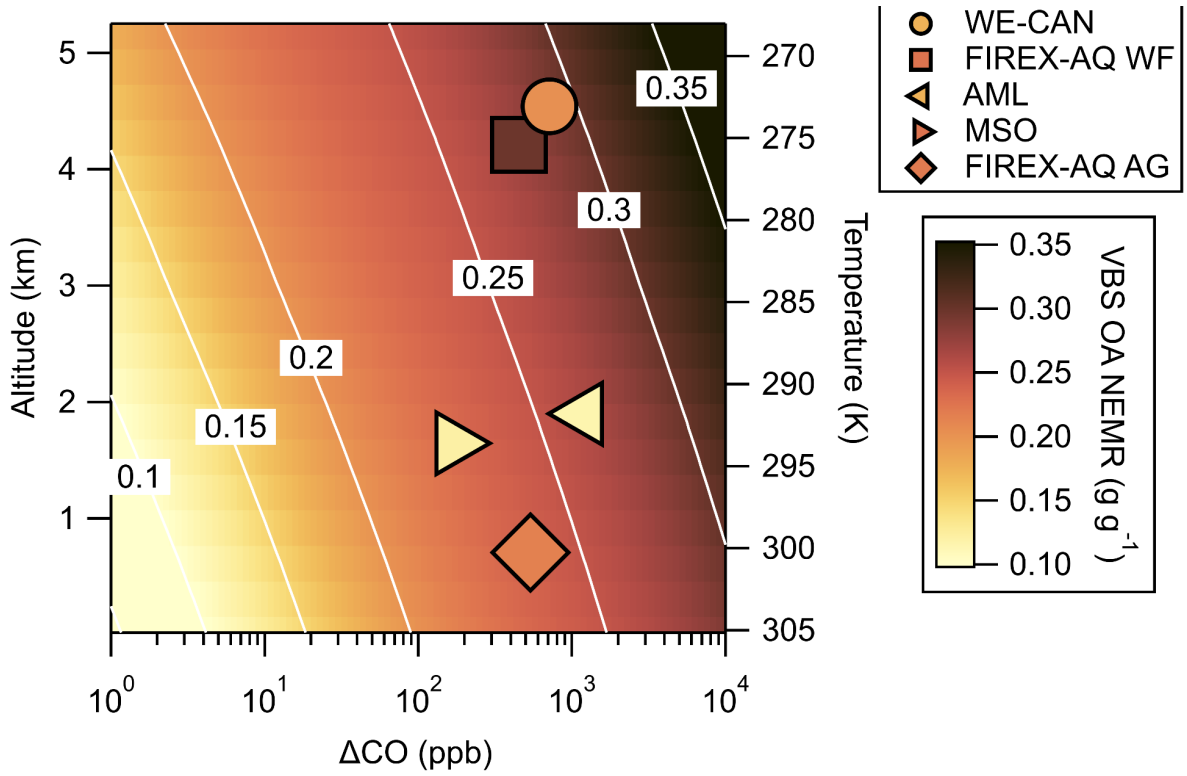

Figure S18. *Relationship between a smoke plume's temperature and concentration and the BBPM NEMR calculated using this work's VBS emission ratios. Each symbol is the average across all data from the indicated platform. Altitude and temperature are interconverted using the standard US tropical atmosphere, since it showed the best correlation with the temperature-altitude profile observed at FIREX-AQ. Airborne campaigns sample at lower temperatures, leading to higher measured NEMR's.*

References

(1) DeCarlo, P. F.; Kimmel, J. R.; Trimborn, A.; Northway, M. J.; Jayne, J. T.; Aiken, A. C.; Gonin, M.; Fuhrer, K.; Horvath, T.; Docherty, K. S.; Worsnop, D. R.; Jimenez, J. L. Field-Deployable, High-Resolution, Time-of-Flight Aerosol Mass Spectrometer. *Anal. Chem.* **2006**, *78* (24), 8281–8289.

(2) Canagaratna, M. R.; Jayne, J. T.; Jimenez, J. L.; Allan, J. D.; Alfarra, M. R.; Zhang, Q.; Onasch, T. B.; Drewnick, F.; Coe, H.; Middlebrook, A.; Delia, A.; Williams, L. R.; Trimborn, A. M.; Northway, M. J.; DeCarlo, P. F.; Kolb, C. E.; Davidovits, P.; Worsnop, D. R. Chemical and Microphysical Characterization of Ambient Aerosols with the Aerodyne Aerosol Mass Spectrometer. *Mass Spectrom. Rev.* **2007**, *26* (2), 185–222.

(3) Nault, B. A.; Campuzano-Jost, P.; Day, D. A.; Schroder, J. C.; Anderson, B.; Beyersdorf, A. J.; Blake, D. R.; Brune, W. H.; Choi, Y.; Corr, C. A.; de Gouw, J. A.; Dibb, J.; DiGangi, J. P.; Diskin, G. S.; Fried, A.; Huey, L. G.; Kim, M. J.; Knote, C. J.; Lamb, K. D.; Lee, T.; Park, T.; Pusede, S. E.; Scheuer, E.; Thornhill, K. L.; Woo, J.-H.; Jimenez, J. L. Secondary Organic Aerosol Production from Local Emissions Dominates the Organic Aerosol Budget over Seoul, South Korea, during KORUS-AQ. *Atmos. Chem. Phys.* **2018**, *18* (24), 17769–17800.

(4) Pagonis, D.; Campuzano-Jost, P.; Guo, H.; Day, D. A.; Schueneman, M. K.; Brown, W. L.; Nault, B. A.; Stark, H.; Siemens, K.; Laskin, A.; Piel, F.; Tomsche, L.; Wisthaler, A.; Coggon, M. M.; Gkatzelis, G. I.; Halliday, H. S.; Krechmer, J. E.; Moore, R. H.; Thomson, D. S.; Warneke, C.; Wiggins, E. B.; Jimenez, J. L. Airborne Extractive Electrospray Mass Spectrometry Measurements of the Chemical Composition of Organic Aerosol. *Atmospheric Measurement Techniques* **2021**, *14* (2), 1545–1559.

(5) Warneke, C.; Schwarz, J. P.; Dibb, J.; Kalashnikova, O.; Frost, G.; Al-Saad, J.; Brown, S. S.; Brewer, W. A.; Soja, A.; Seidel, F. C.; Washenfelder, R. A.; Wiggins, E. B.; Moore, R. H.; Anderson, B. E.; Jordan, C.; Yacovitch, T. I.; Herndon, S. C.; Liu, S.; Kuwayama, T.; Jaffe, D.; Johnston, N.; Selimovic, V.; Yokelson, R.; Giles, D. M.; Holben, B. N.; Goloub, P.; Popovici, I.; Trainer, M.; Kumar, A.; Pierce, R. B.; Fahey, D.; Roberts, J.; Gargulinski, E. M.; Peterson, D. A.; Ye, X.; Thapa, L. H.; Saide, P. E.; Fite, C. H.; Holmes, C. D.; Wang, S.; Coggon, M. M.; Decker, Z. C. J.; Stockwell, C. E.; Xu, L.; Gkatzelis, G.; Aikin, K.; Lefer, B.; Kaspari, J.; Griffin, D.; Zeng, L.; Weber, R.; Hastings, M.; Chai, J.; Wolfe, G. M.; Hanisco, T. F.; Liao, J.; Campuzano Jost, P.; Guo, H.; Jimenez, J. L.; Crawford, J.; The FIREX-AQ Science Team. Fire Influence on Regional to Global Environments and Air Quality (FIREX-AQ). *J. Geophys. Res.* **2023**, *128* (2). https://doi.org/10.1029/2022jd037758.

(6) Garofalo, L. A.; Pothier, M. A.; Levin, E. J. T.; Campos, T.; Kreidenweis, S. M.; Farmer, D. K. Emission and Evolution of Submicron Organic Aerosol in Smoke from Wildfires in the Western United States. *ACS Earth and Space Chemistry* **2019**, *3*, 1237–1247.

(7) Palm, B. B.; Peng, Q.; Fredrickson, C. D.; Lee, B. H.; Garofalo, L. A.; Pothier, M. A.; Kreidenweis, S. M.; Farmer, D. K.; Pokhrel, R. P.; Shen, Y.; Murphy, S. M.; Permar, W.; Hu, L.; Campos, T. L.; Hall, S. R.; Ullmann, K.; Zhang, X.; Flocke, F.; Fischer, E. V.; Thornton, J. A. Quantification of Organic Aerosol and Brown Carbon Evolution in Fresh Wildfire Plumes. *Proc. Natl. Acad. Sci. U. S. A.* **2020**. https://doi.org/10.1073/pnas.2012218117.

(8) Onasch, T. B.; Trimborn, A.; Fortner, E. C.; Jayne, J. T.; Kok, G. L.; Williams, L. R.; Davidovits, P.; Worsnop, D. R. Soot Particle Aerosol Mass Spectrometer: Development, Validation, and Initial Application. *Aerosol Sci. Technol.* **2012**, *46* (7), 804–817.

(9) Collier, S.; Zhou, S.; Onasch, T. B.; Jaffe, D. A.; Kleinman, L.; Sedlacek, A. J., 3rd; Briggs, N. L.; Hee, J.; Fortner, E.; Shilling, J. E.; Worsnop, D.; Yokelson, R. J.; Parworth, C.; Ge, X.; Xu, J.; Butterfield, Z.; Chand, D.; Dubey, M. K.; Pekour, M. S.; Springston, S.; Zhang, Q. Regional Influence of Aerosol Emissions from Wildfires Driven by Combustion Efficiency: Insights from the BBOP Campaign. *Environ. Sci. Technol.* **2016**, *50* (16), 8613–8622.

(10) Liu, X.; Huey, L. G.; Yokelson, R. J.; Selimovic, V.; Simpson, I. J.; Müller, M.; Jimenez, J. L.; Campuzano-Jost, P.; Beyersdorf, A. J.; Blake, D. R.; Butterfield, Z.; Choi, Y.; Crounse, J. D.; Day, D. A.; Diskin, G. S.; Dubey, M. K.; Fortner, E.; Hanisco, T. F.; Hu, W.; King, L. E.; Kleinman, L.; Meinardi, S.; Mikoviny, T.; Onasch, T. B.; Palm, B. B.; Peischl, J.; Pollack, I. B.; Ryerson, T. B.; Sachse, G. W.; Sedlacek, A. J.; Shilling, J. E.; Springston, S.; St. Clair, J. M.; Tanner, D. J.; Teng, A. P.; Wennberg, P. O.; Wisthaler, A.; Wolfe, G. M. Airborne Measurements of Western U.S. Wildfire Emissions: Comparison with Prescribed Burning and Air Quality Implications. *J. Geophys. Res. D: Atmos.* **2017**, *122* (11), 6108–6129.

(11) Liu, X.; Zhang, Y.; Huey, L. G.; Yokelson, R. J.; Wang, Y.; Jimenez, J. L.; Campuzano-Jost, P.; Beyersdorf, A. J.; Blake, D. R.; Choi, Y.; St. Clair, J. M.; Crounse, J. D.; Day, D. A.; Diskin, G. S.; Ried, A.; Hall, S. R.; Hanisco, T. F.; King, L. E.; Meinardi, S.; Mikoviny, T.; Palm, B. B.; Peischl, J.; Perring, A. E.; Pollack, I. B.; Ryerson, T. B.; Sachse, G.; Schwarz, J. P.; Simpson, I. J.; Tanner, D. J.; Thornhil, K. L.; Ullmann, K.; Weber, R. J.; Wennberg, P. O.; Wisthaler, A.; Wolfe, G. M.; Ziemba, L. D. Agricultural Fires in the Southeastern U.S. during SEAC4RS: Emissions of Trace Gases and Particles and Evolution of Ozone, Reactive Nitrogen, and Organic Aerosol. *J. Geophys. Res.* **2016**, *121* (12), 7383–7414.

(12) Selimovic, V.; Yokelson, R. J.; McMeeking, G. R.; Coefield, S. In Situ Measurements of Trace Gases, PM, and Aerosol Optical Properties during the 2017 NW US Wildfire Smoke Event. *Atmos. Chem. Phys.* **2019**, *19* (6), 3905–3926.

(13) Selimovic, V.; Yokelson, R. J.; McMeeking, G. R.; Coefield, S. Aerosol Mass and Optical Properties, Smoke Influence on O 3 , and High NO 3 Production Rates in a Western US City Impacted by Wildfires. *J. Geophys. Res. D: Atmos.* **2020**. https://doi.org/10.1029/2020JD032791.

(14) Moore, R. H.; Wiggins, E. B.; Ahern, A. T.; Zimmerman, S.; Montgomery, L.; Campuzano Jost, P.; Robinson, C. E.; Ziemba, L. D.; Winstead, E. L.; Anderson, B. E.; Brock, C. A.; Brown, M. D.; Chen, G.; Crosbie, E. C.; Guo, H.; Jimenez, J. L.; Jordan, C. E.; Lyu, M.; Nault, B. A.; Rothfuss, N. E.; Sanchez, K. J.; Schueneman, M.; Shingler, T. J.; Shook, M. A.; Thornhill, K. L.; Wagner, N. L.; Wang, J. Sizing Response of the Ultra-High Sensitivity Aerosol Spectrometer (UHSAS) and Laser Aerosol Spectrometer (LAS) to Changes in Submicron Aerosol Composition and Refractive Index. *Atmos. Meas. Tech.* **2021**, *14* (6), 4517–4542.

(15) Cappa, C. D. A Model of Aerosol Evaporation Kinetics in a Thermodenuder. *Atmos. Meas. Tech.* **2010**, *3* (3), 579–592.

(16) May, A. A.; Levin, E. J. T.; Hennigan, C. J.; Riipinen, I.; Lee, T.; Collett, J. L., Jr.; Jimenez, J. L.; Kreidenweis, S. M.; Robinson, A. L. Gas-Particle Partitioning of Primary Organic Aerosol Emissions: 3. Biomass Burning. *J. Geophys. Res. D: Atmos.* **2013**, *118* (19), 11,327–11,338.

(17) Shingler, T.; Crosbie, E.; Ortega, A.; Shiraiwa, M.; Zuend, A.; Beyersdorf, A.; Ziemba, L.; Anderson, B.; Thornhill, L.; Perring, A. E.; Schwarz, J. P.; Campazano-Jost, P.; Day, D. A.; Jimenez, J. L.; Hair, J. W.; Mikoviny, T.; Wisthaler, A.; Sorooshian, A. Airborne Characterization of Subsaturated Aerosol Hygroscopicity and Dry Refractive Index from the Surface to 6.5 Km during the SEAC4RS Campaign: DASH-SP Measurements in SEAC4RS. *J. Geophys. Res. D: Atmos.* **2016**, *121* (8), 4188–4210.

(18) Theodoritsi, G. N.; Ciarelli, G.; Pandis, S. N. Simulation of the Evolution of Biomass Burning Organic Aerosol with Different Volatility Basis Set Schemes in PMCAMx-SRv1.0. *Geoscientific Model Development*. 2021, pp 2041–2055. https://doi.org/10.5194/gmd-14-2041-2021.

(19) Hatch, L. E.; Rivas-Ubach, A.; Jen, C. N.; Lipton, M.; Goldstein, A. H.; Barsanti, K. C. Measurements of I/SVOCs in Biomass-Burning Smoke Using Solid-Phase Extraction Disks and Two-Dimensional Gas Chromatography. *Atmos. Chem. Phys.* **2018**, *18* (24), 17801–17817.

(20) Cappa, C. D.; Jimenez, J. L. Quantitative Estimates of the Volatility of Ambient Organic Aerosol. *Atmos. Chem. Phys.* **2010**, *10* (12), 5409–5424.

(21) Liu, X.; Day, D. A.; Krechmer, J. E.; Brown, W.; Peng, Z.; Ziemann, P. J.; Jimenez, J. L. Direct Measurements of Semi-Volatile Organic Compound Dynamics Show near-Unity Mass Accommodation Coefficients for Diverse Aerosols. *Comm. Chem.* **2019**, *2* (1), 1–9.
(22) Ward, D. E.; Radke, L. F. Emissions Measurements From Vegetation Fires: A Comparative Evaluation of Methods and Results. In *Fire in the Environment: The Ecological, Atmospheric and Climatic Importance of Vegetation Fires*; J, C. P., Goldammer, J. G., Eds.; John Wiley: New York, 1993; pp 53–76.
(23) Fire Influence on Regional to Global Environments and Air Quality. Online Dataset. https://doi.org/10.5067/SUBORBITAL/FIREXAQ2019/DATA001.
(24) Donahue, N. M.; Robinson, A. L.; Stanier, C. O.; Pandis, S. N. Coupled Partitioning, Dilution, and Chemical Aging of Semivolatile Organics. *Environ. Sci. Technol.* **2006**, *40* (8), 2635–2643.